journal

J. Am. Ceram. Soc., 93 [11] 3893–3901 (2010)
DOI: 10.1111/j.1551-2916.2010.03946.x

Compositional Dependence of Phase Formation Mechanisms at the Interface Between Titanium and Calcia-Stabilized Zirconia at 1550°C

Yao-Wen Chang and Chien-Cheng Lin*,†

Department of Materials Science and Engineering, National Chiao Tung University, Hsinchu 30050, Taiwan

ZrO_2 samples with various CaO contents were fabricated by hot pressing, whereby CaO was dissolved by and/or reacted with ZrO_2 to form a solid solution and/or $CaZr_4O_9$, respectively. After a reaction with Ti at 1550°C for 6 h in argon, the interfacial microstructures were characterized using X-ray diffraction and analytical electron microscopy. Experimental results were very different from those found previously in the Y_2O_3–ZrO_2 system. The 5 mol% CaO–ZrO_2 sample was relatively stable due to the formation of a thin TiO layer acting as a diffusion barrier phase. However, α-Ti(O), β′-Ti (Zr, O), and/or Ti_2ZrO were found in 9 or 17 mol% CaO–ZrO_2 due to extensive interdiffusion of Ti, O, and Zr with a much thinner (β′-Ti+α-Ti) layer in 17 mol% CaO–ZrO_2 than in 9 mol% CaO–ZrO_2. Because CaO was hardly dissolved into Ti, it fully remained in the residual ZrO_2, leading to the formation of spherical $CaZrO_3$ in 9 mol% CaO–ZrO_2 and columnar $CaZrO_3$ in 17 mol% CaO–ZrO_2. In the region far from the original interface, abundant intergranular α-Zr was formed in 5 or 9 mol% CaO–ZrO_2. Scattered α-Zr and $CaZrO_3$ were found in 17 mol% CaO–ZrO_2 because a high concentration of extrinsic oxygen vacancies, which were created by the substitution of Ca^{+2} for Zr^{+4}, effectively retarded the reduction of zirconia.

I. Introduction

Because titanium alloys have high tensile strength and toughness, light weight, and extraordinary corrosion resistance, they are widely applied to some parts of aircraft, medical devices, golf club heads, consumer electronics, etc. Titanium alloys are usually melted in a water-cooled copper crucible by the consumable electrode vacuum arc melting (VAR),[1] because the ceramic crucible used in the vacuum induction melting significantly reacts with titanium.[2] However, high cost of the equipment, scrape recycle, and long cycle time are some of drawbacks for the VAR process. Moreover, the reaction between the ceramic mold and titanium parts during invest casting inevitably results in α-casing and the resultant deterioration of mechanical properties. Therefore, how to control the interfacial reactions between titanium and some ceramic materials is of great concerns.

In the past several decades, extensive studies have been performed on the reactions between titanium and zirconia.[3–10] Economos and Kingery[3] found that titanium penetrated along the grain boundaries of ZrO_2 to form black oxygen-deficient zirconia. Ruh[6] indicated that up to approximately 10 mol% zirconia could be dissolved in titanium, while the residual zirconia became oxygen-deficient zirconia. Saha *et al.*[10] also revealed that the oxygen of zirconia was readily extracted and dissolved into the titanium to form α-Ti(O).

Recently, Lin *et al.*[11–15] have thoroughly investigated the phase formation mechanisms and microstructural evolution at the interface between titanium (or titanium alloys) and 3Y–ZrO_2 (or various ratios of Y_2O_3/ZrO_2) using analytical electron microscopy. α-Ti(O), β′-Ti (Zr, O), and/or Ti_2ZrO were formed near the original interface due to the dissolution of ZrO_2 into Ti and vice versa. Both lamellar orthorhombic Ti_2ZrO and spherical hexagonal Ti_2ZrO were found in α-Ti(Zr, O) after reaction at 1550°C.[11] The orientation relations of the acicular α-Ti and the β′-Ti were $[2\bar{1}\bar{1}0]_{\alpha-Ti}//[001]_{\beta'-Ti}$ and $(0001)_{\alpha-Ti}//(100)_{\beta'-Ti}$ in combinations of $[2\bar{1}\bar{1}0]_{\alpha-Ti}//[021]_{\beta'-Ti}$ and $(0001)_{\alpha-Ti}//(1\bar{1}2)_{\beta'-Ti}$, respectively.[13] Lin and Lin[12] also found intergranular α-Zr, twinned t'-ZrO_{2-x}, lenticular t-ZrO_{2-x}, and/or ordered c-ZrO_{2-x} in the zirconia side, far from the interface between Ti and 3Y–ZrO_2 after reaction at 1550°C. Concerning the reaction of the Ti melt with various Y_2O_3/ZrO_2 samples at 1700°C,[15] the incorporation of >30 vol% Y_2O_3 in ZrO_2 could effectively suppress the reactions on the Ti side, where only a very small amount of α-Ti and β′-Ti was found. Furthermore, Y_2O_3 reprecipitated in the samples containing 30–70 vol% Y_2O_3 because the solubility of Y_2O_3 in Ti was very low.

The yttria partially stabilized zirconia (Y-PSZ) has been considered as one of the most popular industrial ceramic materials because of its good fracture toughness. Because Y_2O_3 is much more expensive than CaO or MgO, the zirconia crucibles used in casting industry are frequently made from CaO- or MgO-stabilized zirconia instead. In this study, powder mixtures with various CaO/ZrO_2 ratios were hot pressed and then allowed to react with titanium at 1550°C for 6 h in argon. The reaction layers at the interface were characterized using analytical scanning electron microscopy and analytical transmission electron microscopy. The effect of CaO on the interfacial reactions between Ti and CaO/ZrO_2 samples is elucidated.

II. Experimental Procedures

Starting powders were zirconia (>99.14 wt% ZrO_2+HfO_2, with HfO_2 accounting for approximately 1.84% of this total, <0.5 wt% SiO_2, <0.11 wt% Y_2O_3, <0.08 wt% Na_2O, <0.05 wt% Al_2O_3, <0.05 wt% Fe_2O_3, <0.03 wt% CaO, <0.01 wt% MgO, <0.005 wt% TiO_2, <0.018 wt% U, <0.007 wt% Th; 8.54 μm average particle size; Z-Tech LLC, Bow, NH), and calcia (>99.9 wt% CaO, <0.034 wt% Sr, <0.02 wt% Mg, <0.02 wt% Na, <0.01 wt% K, <0.005 wt% Ba, <0.005 wt% Pb, <0.003 wt% Fe, <0.002 wt% Cd, <0.001 wt% As; 10 μm average particle size; Ube Material Industries Ltd., Chiba, Japan).

The CaO/ZrO_2 samples contained 5, 9, or 17 mol% CaO, with the balance being ZrO_2. The sample consisting of 5 mol% CaO and 95 mol% ZrO_2 was designated as 5C95Z, with the same notation used for the other samples. Powder mixtures were dispersed in ethanol. The pH of the suspension was adjusted to 11 by adding NH_4OH. The suspension was ultrasonically vibrated for 10 min (Model XL-2020, Sonicator, Heat Systems Inc., Farmingdale, NY), dried in an oven at 150°C, ground with

H.-J. Kleebe—contributing editor

Manuscript No. 27356. Received January 8, 2010; approved May 30, 2010.
Research supported by National Science Council of Taiwan under Contract No. NSC 96-2221-E-009-100.
*Member, The American Ceramic Society.
†Author to whom correspondence should be addressed. e-mail: chienlin@faculty.nctu.edu.tw

Table I. Designations, Compositions, Hot-Pressing Conditions, Relative Densities, and XRD Phases of Hot-Pressed CaO/ZrO_2 Samples

Specimens	Composition (mol%)	Hot-pressing conditions	Relative densities (%)	XRD phases
5C95Z	5% CaO+95% ZrO_2	1600°C/30 min/1 atm Ar	98.4	*t*-ZrO_2, *m*-ZrO_2
9C91Z	9% CaO+91% ZrO_2	1600°C/30 min/1 atm Ar	98.9	*c*-ZrO_2, *t*-ZrO_2, *m*-ZrO_2
17C83Z	17% CaO+83% ZrO_2	1600°C/30 min/1 atm Ar	98.0	*c*-ZrO_2, $CaZr_4O_9$

an agate mortar and pestle, and then screened through an 80 mesh. Bulk specimens were fabricated by hot pressing in a graphite furnace at 1 atm argon (Model HP50-MTG-7010, Thermal Technology Inc., Santa Rosa, CA). As hot-pressed samples were blackened and were regarded as oxygen-deficient zirconia. They become stoichiometric after isothermal annealing at 1300°C for 1 h.

The apparent densities of CaO/ZrO_2 powder mixtures were measured using a gas pycnometer (Model MultiVolume Pycnometer 1305, Micromeritics, Norcross, GA) with 99.99% pure helium. Bulk densities of hot-pressed CaO/ZrO_2 samples were determined by the Archimedes method using water as an immersion medium. The relative densities of the hot-pressed samples were calculated as follows: Relative density = (bulk density/true density) × 100%. For a nonporous powder, the apparent density approximates the true density and can be used as the reference point in calculating the relative density. The hot press conditions, compositions, relative densities, and designations of CaO/ZrO_2 samples are listed in Table I.

Commercially pure titanium plates (99.7% purity, Alfa Aesar, Ward Hill, MA) were brought to react with hot-pressed CaO/ZrO_2 samples at 1550°C for 6 h in argon. First, bulk CaO/ZrO_2 samples and titanium plates were cut and machined to dimensions of 10 mm × 10 mm × 5 mm. Their surfaces were ground and polished with a diamond paste and subsequently ultrasonically cleaned in acetone. One titanium specimen was inserted between two pieces of a CaO/ZrO_2 sample to produce a sandwiched type, and the sandwich was then placed into the aforementioned graphite furnace. The furnace was initially prepared by first being pressurized to 5 MPa, then evacuated to 2×10^{-4} torr, and filled with argon to 1 atmospheric pressure. This cycle of evacuation and purging was repeated at least three times. After the sample insertion, the furnace temperature was raised to 1000°C at a heating rate of 30°C/min, to 1550°C at 25°C/min, and then held at 1550°C for 6 h. Thereafter, the temperature was lowered to 1000°C at a cooling rate of 25°C/min, and finally, the furnace was cooled down to room temperature.

The phase identification of the as hot-pressed CaO/ZrO_2 samples was performed using an X-ray diffractometer (XRD, Model MXP18, Mac Science, Yokohama, Japan). The operating conditions of the XRD were Cu*K*α radiation at 50 kV and 150 mA and a scanning rate of 2°/min.

A scanning electron microscope (SEM, Model JSM 6500F, JEOL Ltd., Tokyo, Japan), which was equipped with an energy-dispersive X-ray spectrometer (EDS, Model ISIS 300, Oxford Instrument Inc., London, U.K.), was used for the microstructural observation of the interfaces between Ti and various CaO/ZrO_2 samples. Cross-sectional SEM specimens were cut and ground using standard procedures and finally polished using diamond pastes of 6, 3, and 1 μm in sequence.

The cross-sectional specimens of the interfaces between Ti and various CaO/ZrO_2 samples for transmission electron microscopy (TEM) were prepared by two different methods. Firstly, they were cut perpendicular to the interface and then polished, dimpled, and subsequently ion-beam-thinned using a precision ion-polishing system (PIPS, Model 691, Gatan, San Francisco, CA). The details of this traditional technique for preparing cross-sectional TEM specimens were described in a previous study.[15] Secondly, the TEM samples were acquired by an innovative technique. A specific location on a metallographic sample was ion-bombarded using a focused ion beam (FIB, Model Nova 200, FEI Co., Hillsboro, OR). The FIB operating parameters were adjusted so that the electron beam was 5 kV from 98 pA to 1.6 nA, and the ion beam was 30 kV from 10 pA to 7 nA. A TEM specimen with a thickness of less than 100 nm was electron transparent. The final TEM specimen was approximately 12 μm × 5 μm × 0.05 μm in size.

The interfacial microstructures were then characterized using a TEM (Model JEM 2100, JEOL Ltd.) equipped with an EDS (Model ISIS 300, Oxford Instrument Inc.). Analyses of atomic configurations in various phases were performed using computer simulation software for crystallography (CaRIne Crystallography 3.1, Divergent S.A., Compiegne, France). Chemical quantitative analyses for various phases were conducted by the Cliff–Lorimer standardless technique.[16] A conventional ZAF correction was operated using the LINK ISIS software.

III. Results and Discussion

(1) XRD Analyses

Figure 1 shows the XRD spectra of various hot-pressed CaO/ZrO_2 samples. These spectra are arranged in the sequence of 17C83Z, 9C91Z, and 5C95Z, from top to bottom. Monoclinic $CaZr_4O_9$[17–19] and cubic ZrO_2 were found in the hot-pressed 17C83Z, indicating that cubic ZrO_2 was fully stabilized by 17 mol% CaO. While *c*-ZrO_2, *t*-ZrO_2, and *m*-ZrO_2 were found in 9C91Z, the 5C95Z consisted of *t*-ZrO_2 and *m*-ZrO_2. This indicates that CaO was dissolved by or reacted with ZrO_2 to form a solid solution and/or $CaZr_4O_9$, respectively, in hot-pressed CaO/ZrO_2 samples.

Although Hellmann and Stubican[19] found $Ca_6Zr_{19}O_{44}$ after sintering at 2000°C for 4 h and subsequent prolonged annealing, $Ca_6Zr_{19}O_{44}$ was not found at all in this study. It was noted that few $CaZr_4O_9$ were found in 5C95Z and 9C91Z. Furthermore, only a very small amount of $CaZr_4O_9$ was distributed along the grain boundaries of cubic zirconia in 17C83Z, as illustrated in Fig. 2. It was thus inferred that the equilibrium was not established after hot pressing. X-ray phases of these hot-pressed CaO/ZrO_2 samples are summarized in Table I.

At the eutectoid temperature of $CaO–ZrO_2$ (1140°C),[19] the solid solution of ZrO_2 with more than 17 mol% CaO could decompose into cubic solid solution and two ordered phases (Φ_1: $CaZr_4O_9$,[17–19] and Φ_2:$Ca_6Zr_{19}O_{44}$).[19,20] However, the rates of decomposition to ordered phases are very slow at relatively low temperatures (<1400°C).[19]

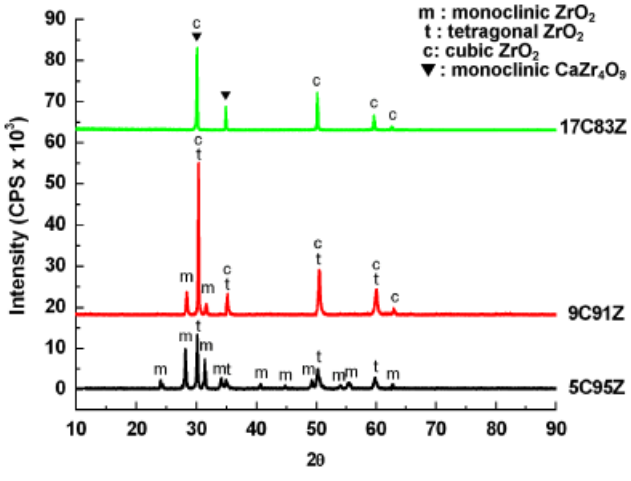

Fig. 1. X-ray diffraction spectra of as hot-pressed CaO/ZrO_2 samples.

(2) SEM and TEM Analyses

Figures 2(a)–(c) display the backscattered electron images of the cross sections normal to the interfaces of Ti and various CaO/ZrO_2 samples. Titanium is shown on the left of the micrograph, while zirconia is on the right-hand side. The vertical arrows on the upper sides of individual figures indicate the original interfaces of Ti and individual CaO/ZrO_2 samples. The original interfaces were deliberately located according to the characteristic K_α X-ray maps of calcium (not shown), which was relatively immobile compared with Zr, O, and Ti. The existence of pores in the ceramic side was attributed to the Kirkendall effect, as zirconium and oxygen diffused to the titanium side much more rapidly than titanium diffused toward the zirconia side.

Figure 2(a) indicates that only a limited reaction occurred on the titanium side at the Ti/5C95Z interface, signifying that interfacial reactions were effectively suppressed. In the engineering respect of Ti castings, a well-controlled interfacial reaction between Ti and 5C95Z can result in a thinner α-casing and thus in better mechanical properties. However, extensive reactions occurred at the Ti/9C91Z and Ti/17C83Z interfaces, as shown in Figs. 2(b) and (c). It was reported previously that needle-like α-Ti and some lamellar phases were usually found in the titanium side because of the interfacial reactions between Ti and $3Y–ZrO_2$.[11,13,14] Even though the system became more stable with the decreasing CaO, several reaction layers were found on the zirconia side after the interfacial reactions between Ti and various CaO/ZrO_2 samples. Microstructures of the reaction layers at the interface between Ti and various CaO/ZrO_2 samples were characterized using SEM/EDS and TEM/EDS, with the results listed in Table II. Four dissimilarities of the interfacial microstructures were recognized after various CaO/ZrO_2 samples reacted with Ti. They are described below.

(A) Two TiO and t-ZrO_2 Layers at the Ti/5C95Z Interface versus Four Complex Layers of α-Ti, β′-Ti, and Ti_2ZrO at the Ti/9C91Z and Ti/17C83Z Interfaces: The two outermost layers were TiO and $t\text{-}ZrO_{2-x}$ layers at the Ti/5C95Z interface. In contrast, the three distinct outermost layers were composed of α-Ti, β′-Ti, and Ti_2ZrO at the Ti/9C91Z or Ti/17C83Z interface. Figure 3(a) shows a bright-field image of a thin TiO reaction layer (about 2 μm thick) at the Ti/5C95Z interface. The arrow indicates the original interface between titanium (α-Ti) and zirconia ($t\text{-}ZrO_{2-x}$). Figures 3(b) and (c) show the selected area diffraction patterns (SADPs) of TiO with [001] and [011] zone axes, respectively. It can be seen that TiO has a B1(NaCl) structure. The EDS spectrum in Fig. 3(d) shows that TiO dissolved a small amount of Zr and was composed of 49.73 at.%

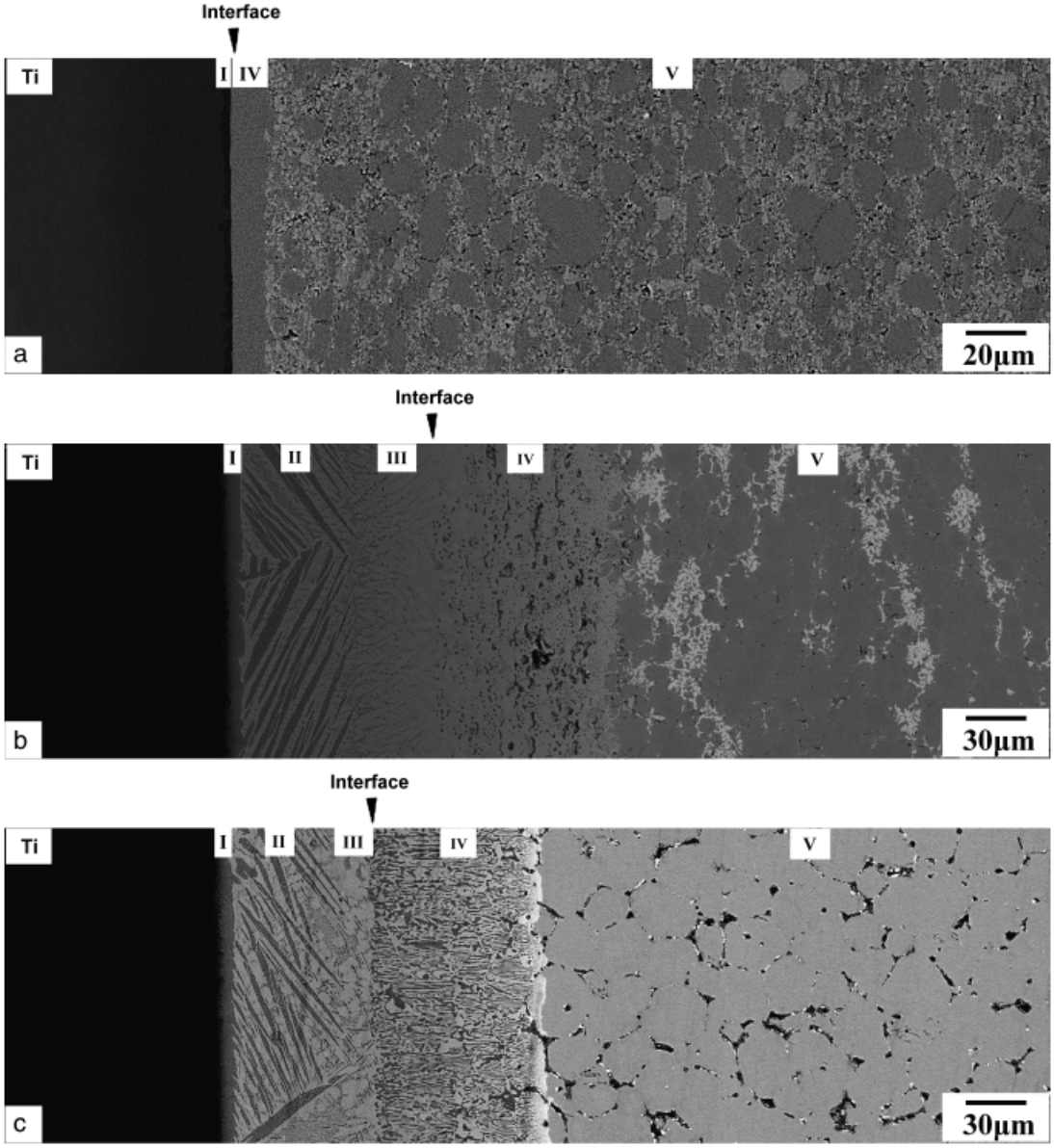

Fig. 2. The backscattered electron images of the interfaces between (a) Ti and 5C95Z, (b) Ti and 9C91Z, and (c) Ti and 17C83Z after reaction at 1550°C for 6 h. The arrows indicate the original interfaces between Ti and CaO/ZrO_2 samples before reaction.

Table II. Thickness and Phases in Various Reaction Layers at the Interfaces of Ti and CaO/ZrO_2 Samples after Reaction at 1550°C for 6 h

	Reaction layers in the titanium side			Reaction layers in the zirconia side		
CaO content (mol%)	Layer	Thickness (μm)	Phases	Layer	Thickness (μm)	Phases
5	I	2	$TiO^{(1)\dagger}$	IV	8	$t\text{-}ZrO_{2-x}^{(1)}$
				V	Very large	$t\text{-}ZrO_{2-x}$, $m\text{-}ZrO_{2-x}$, $\alpha\text{-}Zr^{(1,4)}$
9	I	8	$\alpha\text{-}Ti+Ti_2ZrO^{(1,2)}$	IV	90	$CaZrO_3$, $\beta'\text{-}Ti^{(1,2,3)}$
	II	56	$\alpha\text{-}Ti+Ti_2ZrO+\beta'\text{-}Ti^{(1,2)}$	V	Very large	$c\text{-}ZrO_{2-x}$, $\alpha\text{-}Zr^{(1,4)}$
	III	38	$\beta'\text{-}Ti$+acicular $\alpha\text{-}Ti^{(1,2)}$			
17	I	8	$\alpha\text{-}Ti+Ti_2ZrO^{(1,2)}$	IV	86	$CaZrO_3$, $\beta'\text{-}Ti^{(1,2,3)}$
	II	56	$\alpha\text{-}Ti+Ti_2ZrO+\beta'\text{-}Ti^{(1,2)}$	V	Very large	$c\text{-}ZrO_{2-x}$, $CaZrO_3$, $\alpha\text{-}Zr^{(1,5)}$
	III	14	$\beta'\text{-}Ti$+acicular $\alpha\text{-}Ti^{(1,2)}$			

†Note that the formation mechanisms of various reaction layers are indicated by the superscript numbers in parenthesis: [1]outward diffusion of O; [2]outward diffusion of Zr; [3]inward diffusion of Ti; [4]excluded from ZrO_{2-x}; [5]decomposition of $CaZr_4O_9$.

Ti, 49.26 at.% O, and 1.01 at.% Zr. This indicates that titanium could not dissolve Ca in the solid solution. Figure 3(e) shows the SADP of continuous $t\text{-}ZrO_{2-x}$ phase with a zone axis of [111]. The EDS results indicate that $t\text{-}ZrO_{2-x}$ was composed of 4.96 at.% Ti, 2.72 at.% Ca, 32.62 at.% Zr, and 59.70 at.% O.

Figure 4 shows the backscattered electron image of the reaction layers I and II at the Ti/17C83Z interface. Reaction layer I consisted of α-Ti (dark) and Ti_2ZrO (bright). Reaction layer II consisted of Ti_2ZrO (bright), α-Ti (dark), and β′-Ti (bright). Lin and Lin[11] reported that the Ti_2ZrO lamellae were precipitated from plate-like α-Ti by a eutectoid reaction during cooling. At high temperatures, the primary α-Ti dissolved a significant amount of oxygen and a relatively small amount of zirconium, forming metastable α-Ti, which could result in the precipitation of Ti_2ZrO during cooling. As more Zr was dissolved in α-Ti, β-Ti was formed, some of which was transformed into orthorhombic β′-Ti solid solution during cooling.

(B) A Much Thinner Reaction Layer III (β′-Ti+α-Ti) at the Ti/17C83Z Interface than at the Ti/9C91Z Interface: Figures 2(b) and (c) show a much thinner reaction layer III (β′-Ti+α-Ti) in 17C83Z than in 9C91Z, while their reaction layers (I+II) had approximately the same thickness. Reaction layer III, which dissolved a significant amount of zirconium (β stabilizer) and oxygen (α stabilizer), was composed of α-Ti+β-Ti with Zr and O in solid solution. Lin and Lin[13] indicated that the acicular α-Ti was precipitated from the β′-Ti matrix.

As described in the following section, a stable 1:1 $CaO \cdot ZrO_2$ compound (or $CaZrO_3$) was formed in the ceramic side as Ti and CaO/ZrO_2 samples were brought into contact at 1550°C for 6 h. Assuming that all of CaO was consumed to form $CaZrO_3$, 9C91Z, and 17C83Z had 82 and 66 mol% of excess ZrO_2, respectively. Even though this assumption is not fully correct (i.e., some CaO went into the solid solution of ZrO_2), it was obvious that more excess ZrO_2 existed in 9C91Z than in 17C83Z. As a result, the thinner reaction layer III at the Ti/17C83Z interface was attributed to the fact that a smaller amount of excess ZrO_2 and a relatively large amount of stable $CaZrO_3$ were formed in the outermost ceramic region.

(C) Distinct Morphologies of $CaZrO_3$ in Reaction Layer IV at the Ti/9C91Z and Ti/17C83Z Interfaces: Figure 5 demonstrates the microstructural variations of reaction layers IV at the Ti/9C91Z and Ti/17C83Z interfaces. Both reaction layers IV consisted of $CaZrO_3$ (dark) and β′-Ti (bright). The $CaZrO_3$ phase was sparse and isolated at the Ti/9C91Z interface, while the $CaZrO_3$ phase was dense and interconnected at the 17C83Z interface. As shown in Fig. 5(a), β′-Ti and a relatively small amount of spherical or worm-like $CaZrO_3$ existed in reaction layers IV at the Ti/9C91Z interface. While the excess ZrO_2 was dissolved into Ti at the Ti/9C91Z interface, ZrO_2 reacted with CaO and formed the compound $CaZrO_3$. Figure 5(b) displays the β′-Ti and a relatively large amount of columnar or worm-like $CaZrO_3$ coexisting in reaction layer IV at the

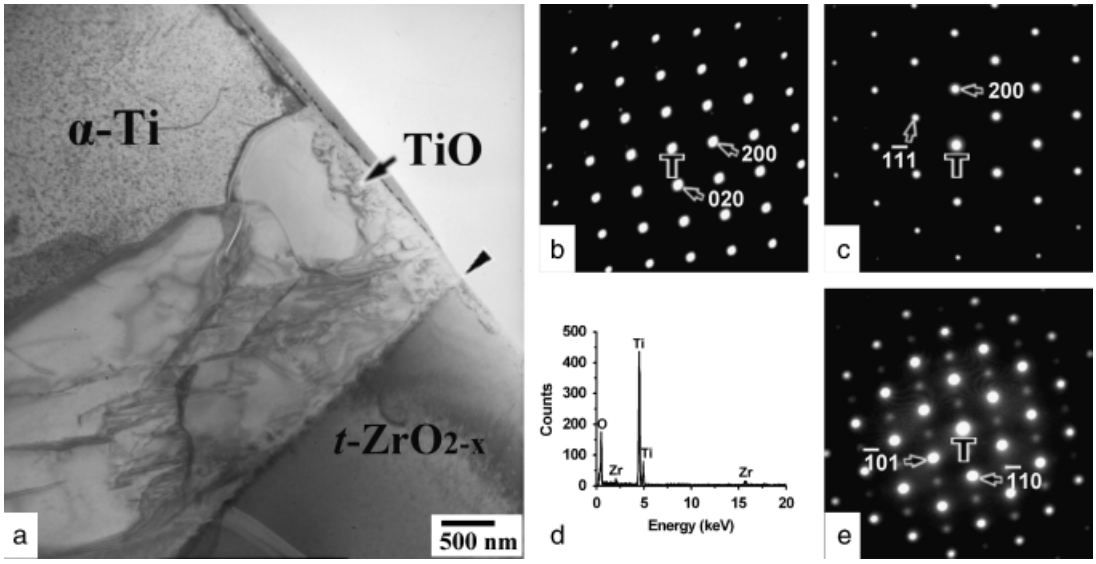

Fig. 3. (a) The bright-field image of reaction layers I and IV at the Ti/5C95Z interface after reaction at 1550°C for 6 h. The arrow indicates the original interface between Ti and 5C95Z before reaction; (b) and (c) selected area diffraction patterns (SADPs) of TiO along the [001] and [011] zone axes, respectively; (d) an energy-dispersive spectrum of TiO; (e) an SADP of $t\text{-}ZrO_{2-x}$ along the zone axis [111].

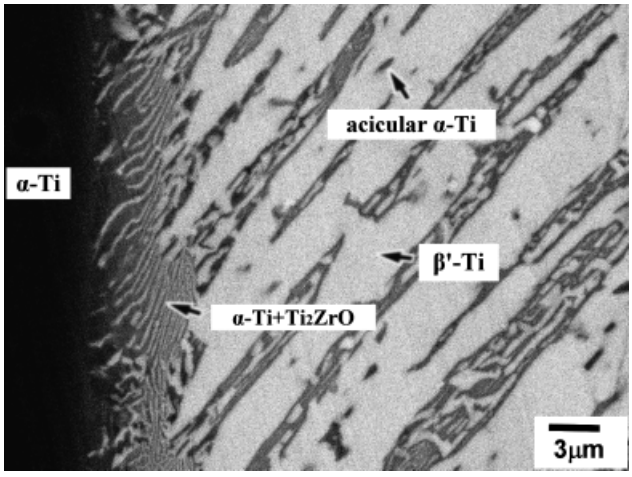

Fig. 4. The backscattered electron image of reaction layers I and II at the Ti/17C83Z interface after reaction at 1550°C for 6 h.

Ti/17C83Z interface. The columnar $CaZrO_3$ was formed due to the outward diffusion of O and Zr away from metastable CaO fully stabilized c-ZrO_{2-x}. This was usually called as a diffusion zone, consisting of β′-Ti and columnar $CaZrO_3$. This result indicates that $CaZrO_3$ was a stable phase and was not significantly dissolved in Ti.

Figure 6(a) shows a bright-field image of reaction layer IV, consisting of β′-Ti and $CaZrO_3$, at the Ti/17C83Z interface. The arrow in the upper right corner indicates the interface between reaction layer IV and reaction layer V. Columnar β′-Ti and $CaZrO_3$ were aligned nearly perpendicular to the interface of reaction layers IV and V. The crystal structures of both $CaZrO_3$ and β′-Ti were identified to be orthorhombic from the superimposed SADPs, as shown in Fig. 6(b). With the diffraction spots being indexed in Fig. 6(b), the orientation relationships of $CaZrO_3$ and β′-Ti were thus recognized as follows: $[101]_{CaZrO_3}//[001]_{\beta'-Ti}$ and $(\bar{1}01)_{CaZrO_3}//(100)_{\beta'-Ti}$. Figure 6(c) shows the EDS spectrum of the $CaZrO_3$, revealing that it comprised 19.93 at.% Ca, 20.61 at.% Zr, and 59.46 at.% O. Figure 6(d) displays the $[101]_{CaZrO_3}$ or $[001]_{\beta'-Ti}$ standard stereographic projection corresponding to the SADPs illustrated in Fig. 6(b). It indicates that the $(\bar{1}01)$ plane of $CaZrO_3$ is parallel to the (100) plane of β′-Ti. Lin and Lin[21] reported that the reaction at 1750°C/7 min between zirconia and titanium melt caused the formation of several $CaZrO_3$ ovals embedded in α-Zr on the zirconia side. No specific orientation relationship was identified in previous studies.

(D) Distinct α-Zr and/or $CaZrO_3$ in Reaction Layer V: Figure 7 displays the backscattered electron images of reaction layer V on the zirconia side far away from the original interfaces. This layer could be termed as a reaction-affected zone. Figure 7(a) displays that dense α-Zr grains existed along the grain boundaries of c-ZrO_{2-x} in reaction layer V of Ti/9C91Z. Dissolution did not play a significant role because the titanium was not detected by EDS in reaction layer V. A much denser α-Zr phase was found at the Ti/5C95Z interface, as shown in Fig. 2(a). In the other respect, very little α-Zr was found in reaction layer V of Ti/17C83Z, as shown in Fig. 7(b). In general, the amount of intergranular α-Zr decreases with the increasing CaO content.

Figures 8(a)–(b) show two bright-field images of reaction layer V on the zirconia side far away from the original interfaces. Figure 8(a) shows the bright-field image of m-ZrO_{2-x}, (t+m)-ZrO_{2-x}, and α-Zr in the reaction layer V of Ti/5C95Z. As 5C95Z reacted with Ti, the metastable oxygen-deficient ZrO_{2-x} was transformed into m-ZrO_{2-x} and α-Zr. Several martensite lathes grew completely across the grain and became twinned m-ZrO_{2-x} (labeled as "m" in Fig. 8(a)) due to the stress concentrations at such a region.[22] Figure 8(b) shows a bright-field image of c-ZrO_{2-x}, $CaZrO_3$, and α-Zr in reaction layer V of Ti/17C83Z. The crystal structure of α-Zr was identified to be hexagonal based upon the superimposed SADP, as shown in the upper right corner. In 17C83Z, ZrO_{2-x} was fully stabilized as a cubic phase because 17 mol% CaO was dissolved into ZrO_2 as a solid solution. This c-ZrO_{2-x} was so stable that no oxidation–reduction was able to occur between zirconia and titanium in reaction layer V. In order to maintain charge neutrality, an oxygen vacancy was created in the crystal lattice of zirconia for every substitution of Ca^{2+} for Zr^{4+}. As a result, there was 17 mol% of oxygen vacancies in 17C83Z if all of the CaO was consumed to form the solid solution of ZrO_2. It was also believed that the intergranular $CaZrO_3$ was found due to the decomposition of intergranular $CaZr_4O_9$ at the Ti/17C83Z interface.

Table II summarizes the formation of various reaction layers at the interface between titanium and various CaO/ZrO_2 samples after reaction at 1550°C for 6 h. The formation mechanisms of α-Ti, β′-Ti, Ti_2ZrO, ZrO_{2-x}, and α-Zr were described in detail previously. However, the following phases were not found in previous studies: (1) TiO and continuous t-ZrO_{2-x} in reaction layers I and IV of Ti/5C95Z; (2) $CaZrO_3$ in reaction layers IV and/or V of Ti/9C91Z and Ti/17C83Z. As also indicated in Table II, the formation mechanisms of various reaction layers are described as follows: (1) reaction layers I, II, and III were formed because of the outward diffusion of O and/or Zr away from zirconia; (2) reaction layer IV was formed because of the inward diffusion of Ti into zirconia together with the outward diffusion of O and Zr away from zirconia; (3) reaction layer V was formed because of the decomposition of metastable oxygen-deficient ZrO_{2-x} and/or $CaZr_4O_9$ as well as the outward diffusion of O away from ZrO_2.

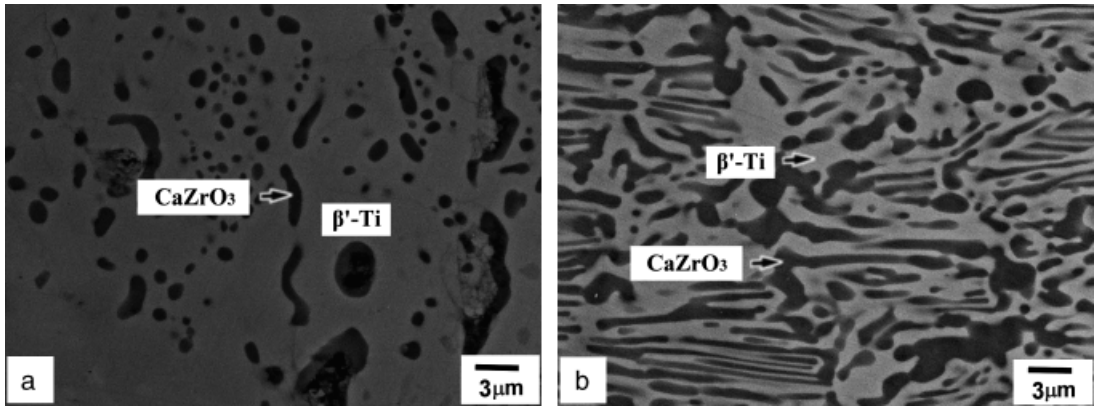

Fig. 5. The backscattered electron images of reaction layer IV at the interface between (a) Ti and 9C91Z, and (b) Ti and 17C83Z after reaction at 1550°C for 6 h.

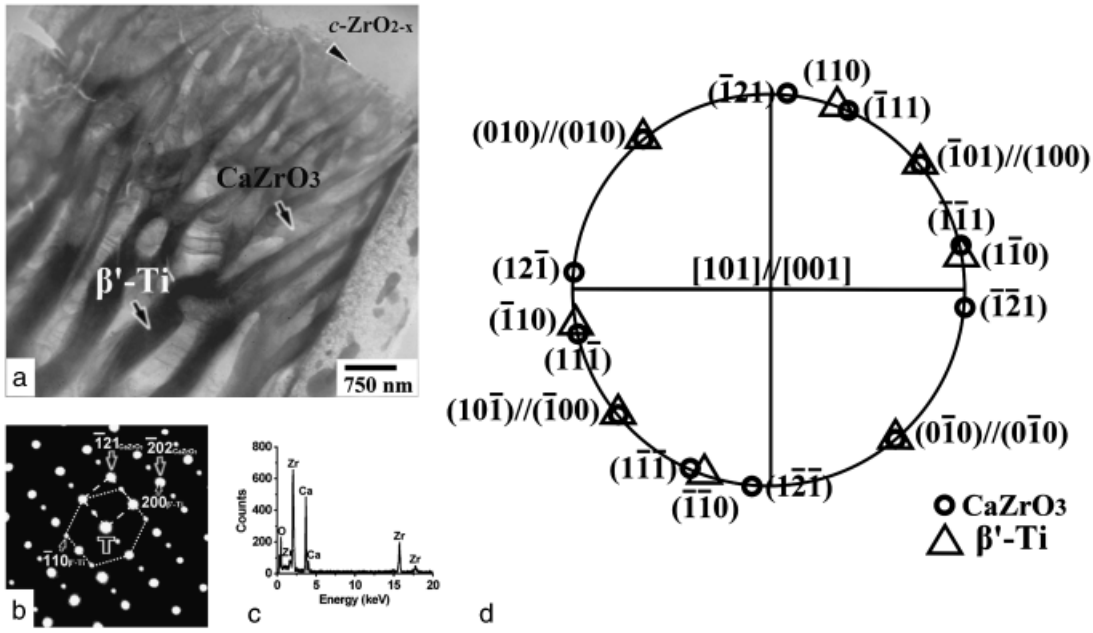

Fig. 6. (a) The bright-field image of reaction layers IV and V at the Ti/17C83Z interface after reaction at 1550°C for 6 h; (b) selected area diffraction patterns of the $CaZrO_3$ and β′-Ti, Z = $[101]_{CaZrO3}//[001]_{\beta'-Ti}$; (c) an energy-dispersive spectrum of $CaZrO_3$; (d) the standard stereographic projection with $[101]_{CaZrO3}//[001]_{\beta'-Ti}$.

(3) Formation Mechanisms of TiO and Continuous t-ZrO_{2-x} at the Ti/5C95Z Interface

As mentioned above, TiO and continuous *t*-ZrO_{2-x} were found in reaction layers I and IV, respectively, at the Ti/5C95Z interface. The TiO reaction layer was formed due to the oxidation–reduction reaction between titanium and zirconia. Previous studies[13,14] reported that α-Ti(O) rather than a TiO layer was observed at the Ti/3Y–ZrO_2 interface after reaction at 1550°C for 6 h. It was inferred that 5 mol% CaO–ZrO_2 released oxygen atoms much more easily than 3Y–ZrO_2 did because the Ca–O bond is weaker than the Y–O bond. This thin TiO reaction layer functioned as a diffusion barrier phase[23] because Ti and Zr diffuse very slowly across the TiO reaction layer, resulting in a suppressed interfacial reaction between Ti and 5C95Z.

While oxygen-deficient zirconia was formed because of the oxidation–reduction between titanium and zirconia, the metastable zirconia with supersaturated oxygen vacancies had the tendency to decompose, leading to the formation of α-Zr along the grain boundaries. However, the dissolution of Ti^{+2} could stabilize the oxygen-deficient zirconia (or ZrO_{2-x}) due to the creation of extra oxygen vacancies. Therefore, continuous *t*-ZrO_{2-x} rather than α-Zr was found in the ceramic outer layer in 5C95Z.

It was noticeable that the TiO layer did not exist at the Ti/9C91Z and Ti/17C83Z interfaces. As mentioned above, almost all CaO and ZrO_2 went into a solid solution in as hot-pressed 9C91Z or 17C83Z. When these metastable solid solutions reacted with Ti at 1550°C, the excess Zr and O had a great tendency to be excluded from the solid solution, with $CaZrO_3$ being left, and subsequently dissolved into Ti. Because TiO had a very limited solubility of Zr as indicated in the ternary phase diagram of Ti–O–Zr,[13,14] the extended dissolution of both Zr and O into Ti (as α-Ti, β′-Ti, and/or Ti_2ZrO) obviously excluded the possibility of the formation of the TiO layer at the Ti/9C91Z and Ti/17C83Z interfaces.

(4) Formation Mechanisms of $CaZrO_3$ and α-Zr at the Ti/9C91Z and Ti/17C83Z Interfaces

Figure 9 shows schematically the formation mechanisms of $CaZrO_3$ and α-Zr at the Ti/9C91Z and Ti/17C83Z interfaces, respectively. Upon heating at 1550°C, the interfacial reactions resulted in the formation of a two-phase (β-Ti+$CaZrO_3$) layer. During cooling, cubic β-Ti was transformed into orthorhombic β′-Ti, where spherical or worm-like $CaZrO_3$ was formed.

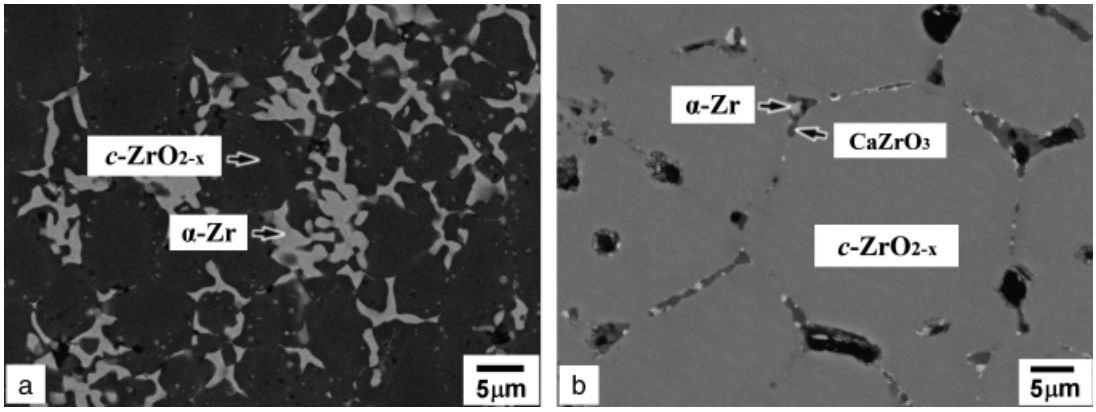

Fig. 7. The backscattered electron images of reaction layer V in the zirconia side, far away from the original interface after reaction at 1550°C for 6 h between (a) Ti and 9C91Z and (b) Ti and 17C83Z.

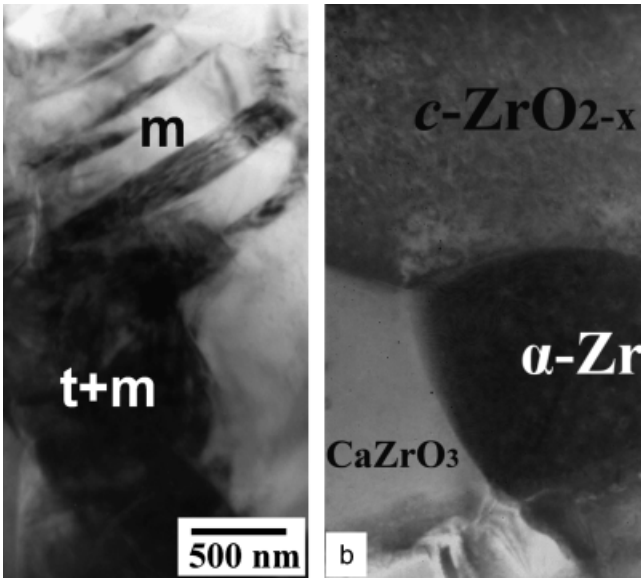

Fig. 8. Bright-field images of reaction layer V in the zirconia side far away from the original interface between (a) Ti and 5C95Z and (b) Ti and 17C83Z after reaction at 1550°C for 6 h. Inset in the upper right hand corner of Fig. 9(b) is a selected area diffraction pattern of α-Zr along the [101] zone axis.

Microstructural evolution in reaction layer IV at the Ti/9C91Z interface is schematically displayed in Fig. 9(a). As 9C91Z reacted with Ti at 1550°C for 6 h, increasing amounts of O and Zr from the CaO–ZrO_2 solid solution were gradually dissolved in titanium. Because CaO remained in the solid solution due to the very limited solubility of CaO in Ti, the increase in the ratio of CaO to ZrO_2 gave rise to the formation of $CaZrO_3$. The formation mechanisms of β′-Ti and $CaZrO_3$ in the case of Ti/9C91Z in the reaction layer IV can be expressed as follows:

$$0.09CaO + 0.91ZrO_2 \rightarrow (Ca_{0.09}Zr_{0.91})O_{1.91} \text{ during hot pressing} \quad (1)$$

$$x - Ti + (Ca_{0.09}Zr_{0.91})O_{1.91} \rightarrow (x - Ti + 0.82Zr + 1.64O) + Ca_{0.09}Zr_{0.09}O_{0.27} \rightarrow \beta' - Ti(Zr, O) + 0.09CaZrO_3 \quad (2)$$

Figure 9(b) displays a proposed model of microstructural evolution in reaction layer IV at the Ti/17C83Z interface. As 17C83Z reacted with Ti at 1550°C for 6 h, titanium diffused into this region and dissolved a relatively small amount of O and Zr, which diffused out of the metastable ZrO_2 phase with supersaturated 17 mol% CaO in solid solution, leading to an appearance of a so-called diffusion zone. As the solubility of Ca in Ti was quite limited, Ca was retained in the residual ZrO_2, causing the formation of columnar $CaZrO_3$. This diffusion zone consisted of a two-phase (β-Ti+$CaZrO_3$) layer and was featured by the columnar $CaZrO_3$ parallel to the diffusion direction. The formation mechanisms of β′-Ti and $CaZrO_3$ in the case of Ti/17C83Z in the reaction layer IV can be expressed as follows:

$$0.17CaO + 0.83ZrO_2 \rightarrow (Ca_{0.17}Zr_{0.83})O_{1.83} \text{ during hot-pressing} \quad (3)$$

$$x - Ti + (Ca_{0.17}Zr_{0.83})O_{1.83} \rightarrow (x - Ti + 0.66Zr + 1.32O) + Ca_{0.17}Zr_{0.17}O_{0.51} \rightarrow \beta' - Ti(Zr, O) + 0.17CaZrO_3 \quad (4)$$

Moreover, as O and Zr diffused out of $CaZr_4O_9$ formed previously during hot pressing, the ratio of CaO/ZrO_2 changed from 1:4 to 1:1. Consequently, $CaZr_4O_9$ was transformed into $CaZrO_3$. This reaction mechanism can be expressed as follows:

$$x - Ti + CaZr_4O_9 \rightarrow (x - Ti + 3Zr + 6O) + CaZrO_3 \rightarrow \beta' - Ti(Zr, O) + CaZrO_3 \quad (5)$$

It is worth mentioning that a columnar $CaZrO_3$ phase was precipitated in 17C83Z from the CaO–ZrO_2 solid solution. As Zr and O of the CaO–ZrO_2 solid solutions in 17C83Z diffused outwards or were selectively dissolved into Ti, the matrix became enriched in CaO. There were two possibilities that $CaZrO_3$ were formed. For example, it might have entered into the two-phase (C_{SS}+$CaZrO_3$) region[18] and then would decompose into *c*-ZrO_2 and $CaZrO_3$ at 1550°C through the nucleation and growth mechanism. However, a diffusion zone was generally featured by columnar precipitates, which grew along the direction parallel to that of diffusion. For instance, Goward and Boone[24] observed a diffusion zone in the aluminized nickel-based superalloys. The morphology of $CaZrO_3$ at the Ti/17C83Z interface implied that it was a diffusion zone and thus excluded the possibility that $CaZrO_3$ was formed through a decomposition process. In other words, the diffusion of Zr and O atoms out of the *c*-ZrO_2 with 17 mol% CaO in solid solution was the primary formation mechanism of the columnar $CaZrO_3$ in the diffusion zone of 17C83Z.

Figure 9(c) illustrates the formation of intergranular α-Zr in reaction layer V of Ti/9C91Z. The oxygen-deficient zirconia entered into a two-phase (α-Zr+ZrO_{2-x}) region[25] because of the oxidation–reduction between Ti and zirconia at such a high temperature as 1550°C. It was obvious that the oxygen-deficient zirconia was metastable because of the supersaturation of oxygen vacancies. The exsolution of Zr from ZrO_{2-x} to the grain boundaries gave rise to the formation of intergranular α-Zr with oxygen in the solid solution.

Figure 9(d) illustrates that less intergranular α-Zr(O) was formed in 17C83Z than in 9C91Z or 5C95Z. The $CaZr_4O_9$ in reaction layer V of Ti/17C83Z could be decomposed into $CaZrO_3$ and α-Zr(O), with O partially dissolved into β′-Ti in reaction layer IV. The decomposition of $CaZr_4O_9$ could be expressed in terms of the following equation:

$$CaZr_4O_9 \rightarrow CaZrO_3 + 3\alpha - Zr_{(\text{with O in solid solution})} + 6O_{(\text{partially dissolved in } \beta' - Ti)} \quad (6)$$

It is also believed that the enthalpy change ΔH for an extra oxygen vacancy significantly increased with the increasing vacancy concentration. While the vacancy concentration increased with the increasing concentration of CaO in the solid solution, the tendency of extraction of oxygen from ZrO_2 by Ti also diminished with the increasing CaO content. It was thus possible that ZrO_{2-x} did not become metastable or oxygen-vacancy supersaturated, so that very little α-Zr was found at the Ti/17C83Z interface.

(5) Thermodynamic Calculation for the Formation of $CaZrO_3$ at the Ti/17C83Z Interface

The metastable solid solution will be decomposed when it is in contact with Ti. The thermodynamic values for the decomposition of 17C83Z are calculated as an example. In addition to four end solid solution phases, there are four intermediate stoichiometric compounds, i.e., *o*-$CaZrO_3$, *c*-$CaZrO_3$, $CaZr_4O_9$(Φ1), and $Ca_6Zr_{19}O_{44}$(Φ2), in the CaO–ZrO_2 binary system.[26] The thermodynamic values acquired were mainly focused on the intermediate compounds $CaZrO_3$ in previous studies,[27–31] while those for the other two intermediate phases (Φ1 and Φ2) are relatively insufficient. It was reported that the intermediate com-

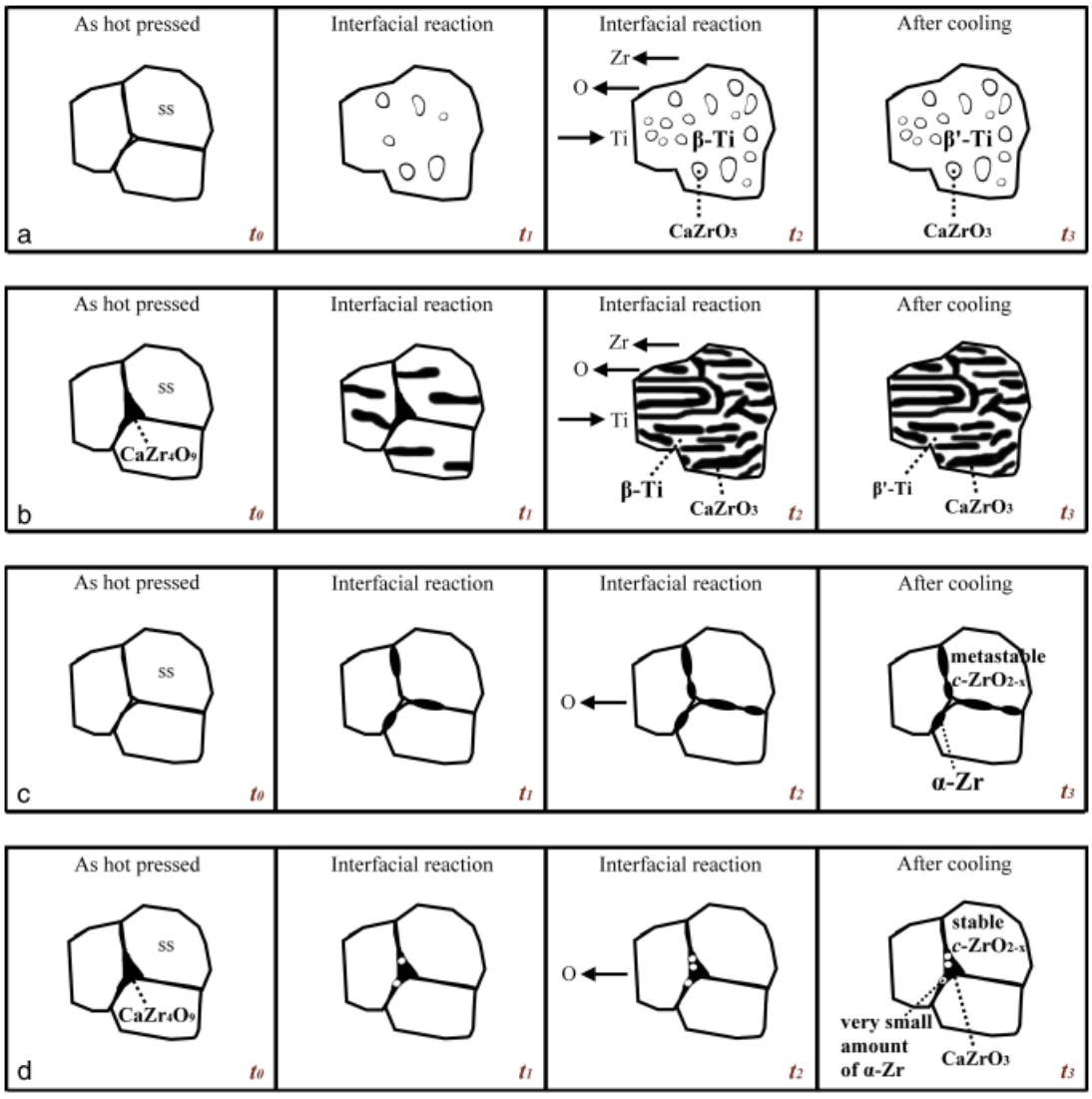

Fig. 9. Schematic diagrams showing the formation mechanisms of (a) $CaZrO_3$ in reaction layer IV at the Ti/9C91Z interface; (b) $CaZrO_3$ in reaction layer IV at the Ti/17C83Z interface; (c) α-Zr in reaction layer V in 9C91Z; (d) α-Zr in reaction layer V in 17C83Z at various intervals ($t_0 < t_1 < t_2 < t_3$). The arrows indicate the diffusion directions for the individual atoms of Ti, Zr, and O assuming that Ti and ZrO_2 are on the left- and right-hand sides, respectively.

pounds Φ1 and Φ2 are stable at the temperatures 1408.5–1507.1 K and 1418.9–1625.6 K, respectively, and *c*-$CaZrO_3$ was stable above 2273 K[32] according to the CaO–ZrO_2 phase diagram proposed by Wang *et al.*[26] Based on these arguments and experimental results, only *o*-$CaZrO_3$ is considered among the four intermediate compounds.

Because of lack of the experimental information for solid solution phases with a wide range of compositions, it is assumed that the decomposition is governed by the following reaction for simplicity. In other words, the 17C83Z solid solution was first decomposed into $CaZrO_3$ and ZrO_2, and then the reduction and dissolution occurred between Ti and ZrO_2

$$\begin{aligned} &0.66\mathrm{Ti} + \mathrm{Ca_{0.17}Zr_{0.83}O_{1.83}} \\ &\rightarrow 0.66\mathrm{Ti} + (0.66\mathrm{ZrO_2} + \mathrm{Ca_{0.17}Zr_{0.17}O_{0.51}}) \\ &\rightarrow 0.66\alpha - \mathrm{TiO}_x + 0.66\mathrm{ZrO_{2-}}_x + 0.17\mathrm{CaZrO_3}\ \Delta G_1 \end{aligned} \quad (7)$$

During hot pressing, ZrO_2 and CaO are mutually dissolved as a homogeneous solid solution phase for the sake of kinetics, which can be expressed as follows:

$$0.17\mathrm{CaO} + 0.83\mathrm{ZrO_2} \rightarrow \mathrm{Ca_{0.17}Zr_{0.83}O_{1.83}}\ \Delta G_2 \quad (8)$$

Using solid electrolyte galvanic cells, the standard Gibbs free energies of formation of $CaZrO_3$ from CaO and ZrO_2 at a different range of temperature were determined. The formation of $CaZrO_3$ can be expressed by the following equation:

$$\mathrm{CaO} + \mathrm{ZrO_2} \rightarrow \mathrm{CaZrO_3}\ \Delta G_3 \quad (9)$$

where $\Delta G_3 = -25.2(\pm 0.15) - 17.58(\pm 0.085) \times 10^{-3} T$ (kJ/mol) and T is the absolute temperature.[28] When $T = 1550°C$ (1823 K), $\Delta G_3 = -57.25$ (kJ/mol), the reduction and dissolution between Ti and ZrO_2 can be expressed by the following equation:

$$\mathrm{Ti} + \mathrm{ZrO_2} \rightarrow \alpha - \mathrm{TiO}_x + \mathrm{ZrO_{2-}}_x\ \Delta G_4 \quad (10)$$

Therefore, $\Delta G_1 = -\Delta G_2 + 0.17\Delta G_3 + 0.66\Delta G_4$. The Gibbs free-energy ΔG_4 can be estimated by taking into consideration the following equivalent defect reaction:

$$\begin{aligned} O^X_{O(\text{in zirconia})} \rightarrow\ & V^{\bullet\bullet}_{O(\text{in zirconia})} + 2e'_{(\text{in zirconia})} \\ & + O''_{i\ (\text{in titanium})} + 2h^{\bullet}_{(\text{in titanium})}\ \Delta G_5 \end{aligned} \quad (11)$$

This equivalent reaction is the combination of dissolution and reduction. Based upon the calculation by Lin and Lin,[12] $\Delta G_5 = \Delta G_{red} + \Delta G_{diss} = 0.54 - 379.30 = -378.76$ (kJ/mol) at 1550°C. Because $\Delta G_4 = x\Delta G_5$, $\Delta G_1 = -\Delta G_2 + 0.17\Delta G_3 + 0.66\, x\Delta G_5$. Substituting $\Delta G_3 = -57.25$ kJ/mol and $\Delta G_5 = -378.76$ kJ/mol, $\Delta G_1 = -\Delta G_2 - 9.73 - 249.98\, x$ (kJ/mol). Because ΔG_2 is a positive value,[33] ΔG_1 must be negative.

Based upon the discussion mentioned above, the formation of $CaZrO_3$ and ZrO_{2-x} induced by the interfacial reaction between Ti and 17C83Z is thermodynamically favorable. This calculation is in good agreement with the present experimental results, indicating the formation of $CaZrO_3$, α-Ti(O), and oxygen-deficient ZrO_{2-x} in layer V. It is believed that extensive diffusion between Ti, Zr, and O is more thermodynamically favorable and results in β′-Ti (O, Zr) and $CaZrO_3$ in layer IV at the Ti/17C83Z interface.

IV. Conclusions

1. The phase formation mechanisms at the interface between Ti and ZrO_2 strongly depended upon the types of stabilizers as well as their amounts. This study shows the promising application of CaO-stabilized-ZrO_2 as molding ceramics for Ti and its alloys while being compared with previous studies conducted on the Ti/Y_2O_3–ZrO_2 interfaces.

2. The 5C95Z shows the best performance due to the formation of a thin layer of TiO, which behaves as a diffusion barrier between Ti and ZrO_2. In other words, the incorporation of 5 mol% CaO into ZrO_2 could effectively suppress the interfacial reactions between Ti and 5C95Z. However, more complex layers consisting of α-Ti, β′-Ti, and Ti_2ZrO were found at interfaces such as Ti/9C91Z and Ti/17C83Z. This indicates that the zirconia with 5 mol% CaO in solid solution is one of the most potential candidates for crucible and mold materials in the Ti-casting industry.

3. Both β′-Ti and spherical $CaZrO_3$ were found at the Ti/9C91Z interface after reaction at 1550°C for 6 h because of extensive dissolution of O and Zr together with a very limited solubility of Ca in Ti.

4. The outward diffusion of Zr and O, which were subsequently dissolved into Ti, gave rise to a diffusion zone featuring columnar $CaZrO_3$ in the matrix of β′-Ti after the reaction between Ti and 17C83Z. This implies that $CaZrO_3$ is a stable phase and thus as a potential refractory when it is taken into contact with titanium alloys at high temperatures.

5. For 5C95Z and 9C91Z, a large amount of α-Zr grains were excluded from metastable oxygen-deficient ZrO_{2-x} on the zirconia side far away from the original interface. In this reaction-affected zone, oxygen-deficient zirconia was partially stabilized as tetragonal in 5C95Z and fully stabilized as cubic in 9C91Z.

6. A very small amount of α-Zr and $CaZrO_3$ was found on grain boundaries of zirconia on the ceramic side far away from the original interface between Ti and 17C83Z. The amount of intergranular α-Zr decreased with the increasing CaO content.

References

[1]G. Broihanne and J. Bannister, "Cold Crucible Melting Gets A New Spin," *Mater. World*, **8** [8] 21–3 (2000).

[2]K. Sakamoto, K. Yashikawa, T. Fujisawa, and T. Onaye, "Changes In Oxygen Contents of Titanium Aluminides by Vacuum Induction, Cold Crucible Induction and Electron Beam Melting," *Iron Steel Inst. Jpn. Int.*, **32** [5] 616–24 (1992).

[3]G. Economos and W. D. Kingery, "Metal–Ceramic Interactions: II, Metal Oxide Interfacial Reactions at Elevated Temperatures," *J. Am. Ceram. Soc.*, **36** [12] 403–9 (1953).

[4]B. C. Weber, H. J. Garrett, F. A. Mauer, and M. A. Schwartz, "Observations on the Stabilization of Zirconia," *J. Am. Ceram. Soc.*, **39** [6] 197–07 (1956).

[5]B. C. Weber, W. M. Thompson, H. O. Bielstein, and M. A. Schwartz, "Ceramic Crucible for Melting Titanium," *J. Am. Ceram. Soc.*, **40** [11] 363–73 (1957).

[6]R. Ruh, "Reaction of Zirconia and Titanium at Elevated Temperatures," *J. Am. Ceram. Soc.*, **46** [7] 301–6 (1963).

[7]A. I. Kahveci and G. E. Welsch, "Effect of Oxygen on the Hardness and Alpha/Beta Phase Ration of Ti–6Al–4V Alloy," *Scr. Metall.*, **20** [9] 1287–90 (1986).

[8]R. L. Saha and K. T. Jacob, "Casting of Titanium and It's Alloy," *Def. Sci.*, **36** [2] 121–41 (1986).

[9]K. I. Suzuki, S. Watakabe, and K. Nishikawa, "Stability of Refractory Oxides for Mold Material of Ti–6Al–4V Alloy Precision Casting," *J. Jpn. Inst. Met.*, **60** [8] 734–43 (1996).

[10]R. L. Saha, T. K. Nandy, R. D. K. Misra, and K. T. Jacob, "On the Evaluation of Stability of Rare Earth Oxides Face Coats for Investment Casting of Titanium," *Metall. Trans.*, **21B** [6] 559–66 (1990).

[11]K. L. Lin and C. C. Lin, "Ti_2ZrO Phases Formed in the Titanium and Zirconia Interface after Reaction at 1550°C," *J. Am. Ceram. Soc.*, **88** [5] 1268–72 (2005).

[12]K. L. Lin and C. C. Lin, "Zirconia-Related Phases in the Zirconia/Titanium Diffusion Couple after Annealing at 1100° to 1550°C," *J. Am. Ceram. Soc.*, **88** [10] 2928–34 (2005).

[13]K. L. Lin and C. C. Lin, "Microstructural Evolution and Formation Mechanism of the Interface Between Titanium and Zirconia Annealed at 1550°C," *J. Am. Ceram. Soc.*, **89** [4] 1400–8 (2006).

[14]K. L. Lin and C. C. Lin, "Effects of Annealing Temperature on Microstructural Development at the Interface Between Zirconia and Titanium," *J. Am. Ceram. Soc.*, **90** [3] 893–9 (2007).

[15]C. C. Lin, Y. W. Chang, and K. L. Lin, "Effect of Yttria on Interfacial Reactions Between Titanium Melt and Hot-Pressed Yttria/Zirconia Composites at 1700°C," *J. Am. Ceram. Soc.*, **91** [7] 2321–7 (2008).

[16]G. Cliff and G. W. Lorimer, "The Quantitative Analysis of Thin Specimens," *J. Microsc.*, **130** [3] 203–7 (1975).

[17]R. C. Garvie, "The Cubic Field in the System ZrO_2–CaO," *J. Am. Ceram. Soc.*, **51** [10] 553–6 (1968).

[18]V. S. Stubican and S. P. Ray, "Phase Equilibria and Ordering in the System ZrO_2–CaO," *J. Am. Ceram. Soc.*, **60** [11–12] 534–7 (1977).

[19]J. R. Hellmann and V. S. Stubican, "Stable and Metastable Phase Relations in the System ZrO_2–CaO," *J. Am. Ceram. Soc.*, **66** [4] 260–4 (1983).

[20]J. R. Hellmann and V. S. Stubican, "The Existence and Stability of $Ca_6Zr_{19}O_{44}$ Compound in the System ZrO_2–CaO," *Mater. Res. Bull.*, **17** [4] 459–65 (1982).

[21]K. F. Lin and C. C. Lin, "Interfacial Reactions between Zirconia and Titanium," *Scr. Metall.*, **39** [10] 1333–8 (1998).

[22]A. H. Heuer and M. Ruhle, "On the Nucleation of the Martensitic Transformation in Zirconia (ZrO_2)," *Acta Metall.*, **33** [12] 2101–12 (1985).

[23]H. Hao, Y. Wang, Z. Jin, and X. Wang, "Joining of Zirconia Ceramic to Stainless Steel and to Itself Using $Ag_{57}Cu_{38}Ti_5$ Filler Metal," *J. Am. Ceram. Soc.*, **78** [8] 2157–60 (1995).

[24]G. W. Goward and D. H. Boone, "Mechanisms of Formation of Diffusion Aluminide Coatings on Nickel-Base Superalloys," *Oxid. Met.*, **3** [5] 475–95 (1971).

[25]R. F. Domagala, S. R. Lyon, and R. Ruh, "The Pseudobinary Ti–ZrO_2," *J. Am. Ceram. Soc.*, **56** [11] 584–7 (1973).

[26]K. Wang, C. H. Li, Y. H. Gao, X. G. Lu, and W. Z. Ding, "Thermodynamic Reassessment of ZrO_2–CaO System," *J. Am. Ceram. Soc.*, **92** [5] 1098–104 (2009).

[27]G. Roga and M. Potoczek-Dudek, "Determination of the Standard Molar Gibbs Energy of Formation of Calcium Zirconate by a Galvanic Cell Involving Calcium-Ion Conducting Solid Electrolyte," *J. Chem. Thermodyn.*, **33**, 77–82 (2001).

[28]J. Tanabe and K. Nagata, "Use of Solid-Electrolyte Galvanic Cells to Determine the Activity of CaO in the CaO–ZrO_2 System and the Standard Gibbs Free Energies of Formation of $CaZrO_3$ from CaO and ZrO_2," *Metall. Mater. Trans. B*, **27B** [8] 658–62 (1996).

[29]K. T. Jacob and Y. Waseda, "Gibbs Energy of Formation of Orthorhombic $CaZrO_3$," *Thermochim. Acta*, **239**, 233–41 (1994).

[30]B. R. Brown and K. O. Bennington, "Thermodynamic Properties of Calcium Zirconate," *Thermochim. Acta*, **106**, 183–90 (1986).

[31]V. A. Levitski, P. B. Narchuk, Ju. Hekimov, and J. I. Gerassimov, "Thermodynamic Study of Some Solid Solutions in CaO–ZrO_2 System by EMF Method," *Solid State Chem.*, **20**, 119–25 (1977).

[32]E. R. Andrievskaya, A. V. Shevchenko, L. M. Lopato, and Z. A. Zaitseva, "Interactions in the System $CaZrO_3$–Y_2O_3," *Izv. Akad. Nauk SSSR Neorg. Mater.*, **25** [9] 1338–40 (1989).

[33]K. S. Mohandas and D. J. Fray, "Electrochemical Deoxidation of Solid Zirconium Dioxide in Molten Calcium Chloride," *Metall. Mater. Trans. B*, **40B** [10] 685–99 (2009). □